Construction and Building Materials 155 (2017) 919–929

Contents lists available at ScienceDirect

Construction and Building Materials

journal homepage: www.elsevier.com/locate/conbuildmat

Innovation for evaluating aggregate angularity based upon 3D convolutional neural network

Zheng Tong [a,b], Jie Gao [a], Haitao Zhang [b,*]

[a] School of Highway, Chang'an University, Xi'an 710061, China
[b] College of Civil Engineering, Northeast Forestry University, Harbin 150040, China

HIGHLIGHTS

- A self-developed device for acquiring aggregate images was developed, 6 × 6 sized kernels were selected as way to evaluate AI.
- Sensitivity analysis to images solutions showed that there was no significant influence of images solutions in range of 72–300 PPI.
- AI CNN with 6 × 6 sized kernels was most acceptable for its relative error.

ARTICLE INFO

Article history:
Received 4 March 2017
Received in revised form 24 June 2017
Accepted 22 August 2017
Available online 23 September 2017

Keywords:
Aggregate angularity
Aggregate index
Convolutional neural network
Image processing
Sensitivity analysis

ABSTRACT

The performance of asphalt pavement is significantly influenced by the morphological characteristics of its aggregates, especially on its angularity. Evaluation of aggregate angularity is considered to be challenging because aggregates often have various shapes. Therefore, utilization of digital images in the evaluation of angularity has gained significant research interest in recent years. However, conventional manually processed images for evaluating the angularity of aggregates have the disadvantages of low efficiency and insufficient accuracy. This paper presents a novel application of convolutional neural networks (CNN) using digital images for evaluating aggregate angularity automatically. The research procedure is as follows: (a) develop a self-developed device for the acquisition of aggregate images; (b) establish an evaluation criterion for the angularity index (AI); (c) design a localization CNN and five AI CNNs; and (d) conduct a sensitivity analysis of the CNNs. First, a self-developed device is established based on the view-based approach to extract the 3D information of aggregates. Then, an evaluation criterion that is suitable for 3D images from aggregates is presented. Based on the 3D images and evaluation criterion, one localization CNN and five AI CNNs are jointly used to evaluate the AI of each aggregate. Finally, statistical analysis is performed to seek the optimal parameters for AI CNN, especially the kernel size, and to verify the sensitivity of AI CNN. The analysis includes the sensitivity to kernels size, image resolution, light, texture and aggregate size. The results indicate that the localization CNN is able to locate and abstract each aggregate from the images. The best size of the kernels is 6 × 6, and an AI CNN with a kernel size of 6 × 6 has a 0.0938 relative error for evaluating the AI using 300 PPI images. Moreover, AI CNN with a kernel size of 6 × 6 shows remarkable robustness under different light conditions, sizes and textures of aggregates.

1. Introduction

The performances of asphalt pavements largely depend on the morphology of coarse aggregates which mainly include its angularity, texture and shape [1,2]. Aggregate angularity, which reflects the convexity degrees of aggregate, is responsible for providing superior rutting resistance in asphalt pavements to improve the shear strength properties of hot-mix asphalt and unbound aggregate base layers [3,4]. Since the aggregate angularity directly affects the performance of pavement, such as the dosage of binder, dynamic modulus, and high temperature stability [5–7], it is meaningful to develop a reliable and precise method to evaluate and control aggregate angularity timely. However, the standards used to evaluate aggregate angularity mainly rely on human operation and their experiences, which have disadvantages of hysteretic and subjective natures [8–10].

* Corresponding author.
E-mail address: zht6781@163.com (H. Zhang).

http://dx.doi.org/10.1016/j.conbuildmat.2017.08.129
0950-0618/

In recent years, several innovative technologies have been used to evaluate aggregate angularity, such as laser technique, X-ray and digital imaging technique (DIT). Comparatively, DIT has the advantage of low cost with high efficiency. Therefore, DIT has been widely used to evaluate aggregate angularity, such as the Aggregate Image System (AIMS) [11] and the University of Illinois Aggregate Image Analyzer (UIAIA) [12]. In addition, some modified algorithms have been introduced to DIT to improve its accuracy. For example, Chen et al. [13] used the Sobel operation to evaluate aggregate angularity. Meanwhile, comparing the results of 1-pixel and 2-pixel, a modified Sobel operation was put forward to improve the robustness of this algorithm. Bian et al. [14] evaluated the aggregate morphology via a three-dimensional modeling system quantitatively. It turned out that this image-based modeling technique, which used two planar mirrors, was an effective way to evaluate the morphological properties of coarse aggregates, and this method could quantitatively analyze some essential parameters of aggregates such as F&E ratio angularity index.

Although the methods above could evaluate aggregate angularity using digital images, some problems remain: (1) the two-dimensional images and formulas could not completely reflect the aggregate angularity; (2) the algorithm robustness can be affected by the poor light conditions; (3) some human assistance is required to locate the aggregates in digital images. Therefore, it is a key research issue to develop three-dimensional images based the aggregate angularity evaluation system, which possess enough robustness towards different light conditions, sizes and textures of aggregates.

With the development of computational ability, graphics devices and mobile-networks, convolutional neural network (CNN) has the capability of handling 3D images effectively. For example, Leng et al. [15] utilized deep hierarchy architecture to recognize 3D subjects, and Ji et al. [16] developed a novel 3D CNN model for action recognition. This model extracted features from both the spatial and temporal dimensions by performing 3D convolutions, thereby capturing the motion information encoded in multiple adjacent frames. In addition, CNN has also been used in the fields of audio classification [17], image restoration [18], denoising [19], and segmentation tasks [20], in which all yielded competitive performance. From the above-mentioned references, CNN was invoked as a class of machines that could learn a hierarchy of features by building high-level features from low-level ones. With the Euclidean Loss Layer for CNN advancing in Caffe, the regression calculation was realized so that subjects' features could be quantified. In addition, CNN showed strong performance in its filtering capacity to background noise, which could be applied to eliminate the influence of shadows. However, there has been little research performed on aggregate angularity.

Therefore, attempts are made to employ the 3D-CNN method to provide an appropriate model for evaluating aggregate angularity automatically with time based on digital images. First, a self-developed device for acquiring aggregate images is developed based on the view-based approach. Then, an evaluation criterion of AI characterization is put forward considering the 3D features of aggregates. Based on the evaluation criterion, one localization CNN and five AI CNNs are realized. Finally, sensitivity analysis is performed to confirm the best parameters of AI CNNs.

2. Research approaches

Fig. 1 shows the main research procedure in this paper. To prepare the training and testing samples, a self-developed device was developed based on the view-based approach. Meanwhile, an evaluation criterion of AI characterization was put forward to obtain the target samples. One localization CNN and five AI CNNs with different sized kernels, i.e., 2×2, 4×4, 6×6, 8×8, 10×10, were realized based on these samples. Due to the numerous factors influencing the results of AI CNNs, a statistical analysis was presented for seeking the optimal AI CNN parameters and verifying the sensitivity of AI CNN. The analysis included sensitivity to sizes of kernels, image resolution, light, texture and size of aggregates. At last, the best parameters and robustness of AI CNNs were discussed based the results of the statistical analysis.

2.1. 3D feature detection for aggregate

The first step of developing a 3D aggregate angularity evolution model was to extract information to reflect the angularity features in specific methods. Generally speaking, methods for 3D object feature extraction are divided into model-based and view-based approaches. Model-based methods detect the features directly from the original 3D object with the topological and geometric information [21,22]. View-based methods [23,24] first capture some 2D views from the original object with some fixed viewpoints and then consider these view images as the information of the object. As shown by references [25–27], some mature methods could be utilized in image processing to process these view images and extract discriminative characteristics from them in view-based methods. For instance, in reference [25], the global shape similarity between two 3D models was achieved by applying a novel matching scheme, which effectively combined the information extracted from the multi-view representation. Moreover, Gao [26] constructed multiple hypergraphs for a set of 3D objects based on their 2D views. In addition, Leng et al. [27] used view-based methods to recognize 3D subjects by 3D CNN. Analogously, to utilize CNN to evaluate AI, the view-based method was employed in this research due to their flexibility and good performance.

Based on the view-based approach, a self-developed device for acquiring aggregate images was developed. The device mainly included three digital image cameras with fixed viewpoints and two light-emitting diodes (LED). The details of the device are shown in Fig. 2. As shown in Fig. 2, aggregates were put in the plane, which had two LEDs on its two sides. LEDs were adopted to simulate the actual working conditions with different light intensities based on illumination, whose range was 0.1–1000 *lx*. Remarkably, the range of 0.1–1000 *lx* was divided into ranges of 400–1000 *lx*, 100–400 *lx* and 0.1–100 *lx* and named as bright, medium and dark conditions, respectively. The three different lighting conditions were used in the sensitivity analysis to light in the follow-up work. Three digital image cameras were installed on the plane. The three digital image cameras were in fixed viewpoints to guarantee that the images acquired had the same viewing angle. As shown in Fig. 2, the lens of the digital image camera in the middle was kept perpendicular to the plane, while the lenses of the digital image cameras on the two sides were kept at a fixed angle (30°) with the viewing angle of the digital image camera in the middle. These three cameras were connected with a computer, which controlled the parameters of the cameras, such as image resolution. Images with different viewpoints were acquired using the device and were used as the training and testing samples for CNNs. The image acquisition process was as follows.

Step1: put 20 aggregates in the plane of the self-developed device;
Step2: select the light intensity to be in the range of 0.1–100 *lx* by changing the light of two LEDs and select a resolution of 300 pixels per inch (PPI) by setting the parameters of the computer;
Step3: acquire aggregate images with different viewpoints using three digital image cameras;
Step4: select the resolutions of 180 PPI, 72 PPI, 54 PPI, and 36 PPI and repeat Step 3.

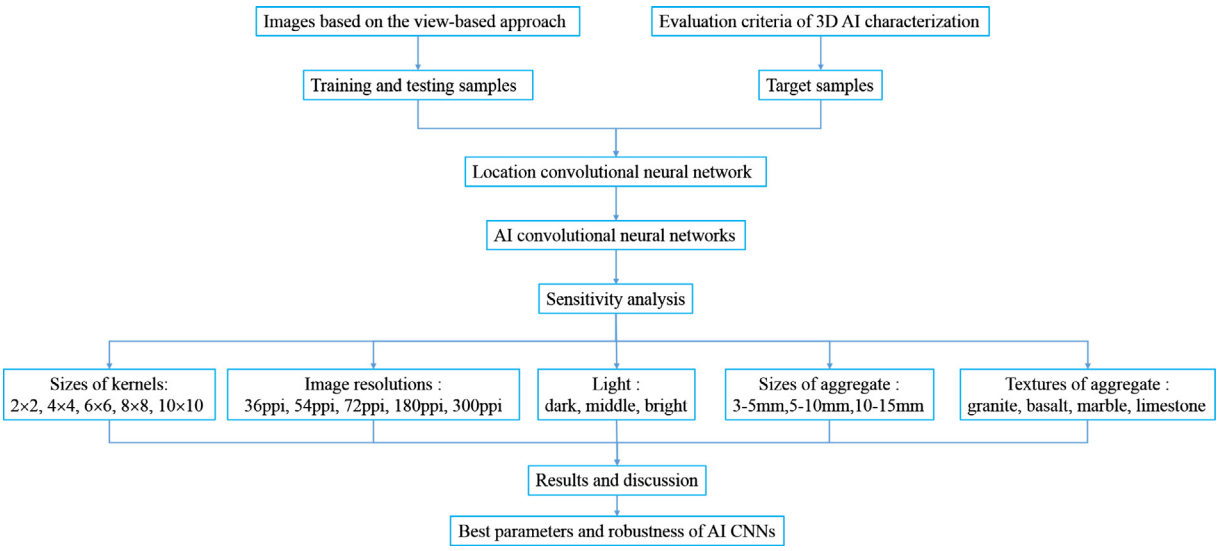

Fig. 1. Flow chart of CNN system.

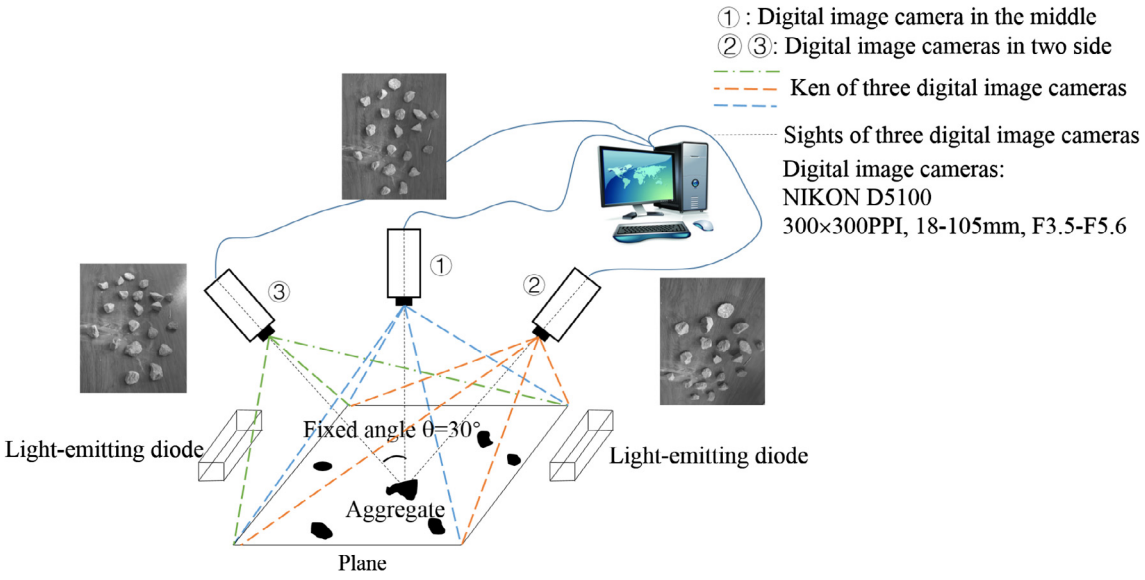

Fig. 2. Device for image capturing.

Step5: select the light intensity to be in the ranges of 100–400 *lx* and 400–1000 *lx* and repeat Step 3 and Step4;
Step6: put another 20 aggregates in the plane of the self-developed device and repeat Steps 1–5.

One group of images includes three different viewpoints, as shown in Fig. 2. Obviously, the aggregate angularities on different sides were reflected clearly.

2.2. AI characterization

To utilize 3D images to define or quantify the aggregate angularity, an evaluation criterion of 3D angularity index (AI) characterization was put forward based on the research of Rao et al. [28]. In the research of Rao et al., the angularity was evaluated in three directions (top, side and front view) based on the images. Then, the AI was calculated by averaging the results of all three views. However, the aggregates were kept out of each other in the side viewpoints. Thus, the self-developed device was more reasonable for detecting several aggregates at the same time. The results of AI calculated by our evaluation criterion were used as the target samples in the training and truth data to validate and test our developed CNNs in the test. The steps to calculate the AI value of an aggregate were as follows.

Step 1: Draw an n-sided polygon (Fig. 3a) as the particle outline in a viewpoint; this was done by dividing the perimeter of the particle into n equal segments;
Step 2: Compute the angle at each vertex of the polygon. These angles were identified as, α_1, α_2, α_3,..., α_n at vertices 1, 2, 3,..., n, respectively (Fig. 3a);
Step 3: Estimated the relative change in the slope of the n sides of the polygon by computing the change in angle at each vertex with respect to the angle in the preceding vertex. The changes in angles β_1, β_2,..., β_n are computed, where $\beta_1 = (\alpha_1 - \alpha_2)$, $\beta_2 = (\alpha_2 - \alpha_3)$,..., $\beta_n = (\alpha_n - \alpha_1)$;
Step 4: Establish the frequency distribution of the changes in the vertex angles, β_1, β_2,..., β_n, which was d in 10° class intervals

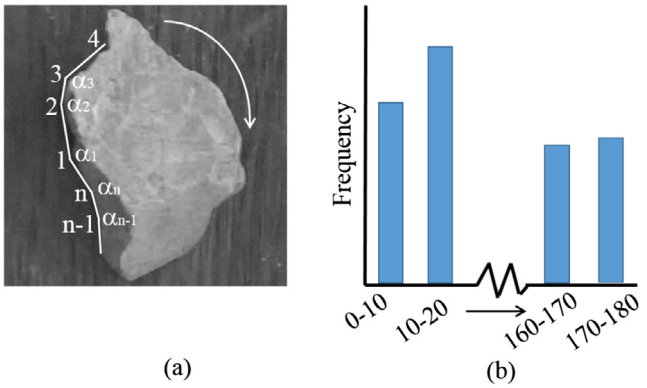

Fig. 3. Angularity determination for a two-dimensional aggregate image.

as shown in Fig. 3b. The distribution of the β values, i.e., the number of occurrences in a certain interval and the magnitude, was now related to the angularity of the particle profile.
Step 5: Calculate the angularity by formula (1).
Step 6: Calculate the angularities in the other two viewpoints by formula (1) by repeating Steps 1–5.
Step 7: Calculate the AI by our modified means for three viewpoints via formula (2). Notably, the AI was distorted in the images of two side viewpoints. To overcome these distortions, a correction factor 1.05 was proposed to perfect Rao's formula based on the value of θ.

From the procedure described above, with the increment of AI, the aggregate had a large angularity. The unit of AI is °.

Then, a correlation between images and formulas should be put forward to evaluate the AI by the images directly. From the research of Rao et al. [28], the algorithms took a long time to evaluate the AI in actual working conditions for approximating the particle outline by an n-sided polygon by hand. In addition, in references [13,14], AI was computed by their algorithms directly. Thus, the results of AI were influenced by the shade of aggregates in different light conditions and the size and texture of aggregates. Clearly, it is too difficult to consider all factors to remove the negative influence of light, sizes and textures by unsupervised algorithms. Thus, as a supervised algorithm, deep learning, to be more precise, CNN, was adopted to overcome the problems mentioned above.

$$Angularity(i) = \sum_{e=0}^{170} e \times P(e) \tag{1}$$

$$AI = Angularity(top) + \frac{1.05 \times [Angularity(side1) \times Area(side1) + Angularity(side2) \times Area(side2)]}{Area(side1) + Area(side2)} \tag{2}$$

where

e — the starting angle for each 10-degree class interval,
$P(e)$— the frequency of change in angle which has a value in the range of e to (e+10),
$Angularity(i) - Angularity(top), Angularity(side1),$
$Angularity(side2)$ obtained from three digital image cameras.

2.3. Convolutional neural network

To date, deep learning has attracted great attention and has been widely used in many fields with excellent performance in representing 3D object information [15,16]. Deep learning is designed to simulate the human neural nervous system, which has been considered as a promising model to extract and represent the 3D features of objects.

Convolutional neural networks (CNN) as a widely used deep learning has two special connections: convolution and pooling. For convolution, it needs to slide a sub-window called convolution kernel in a 2D image from the left-upper corner to the right-down corner to conduct the image convolution. As a result, the image can be divided into a number of overlapping sub-windows for extracting features from images. A CNN has several kernels, which can extract different features from images. The parameters are shared by the sub-windows in each kernel, but are different internally. The activating function of convolution used in this paper is shown in formulas (3) and (4). For pooling, there are usually two types of operations: max pooling and averaging pooling. For images, if the maximal value is obtained as the result, it is max pooling, and if the block is averaged, it is averaging pooling. In this research, max pooling was used in each CNN.

$$I_{ij}^{k} = f\left(\sum_{r,c=0}^{N} I_{ij}^{k-1} W_{r,c}^{k} + b^{k}\right) \tag{3}$$

$$f(x) = max(0, x) \tag{4}$$

where

$W_{r,c}^{k}$ — the weight parameters between two convolution layers,
N_w — size of kernels,
b — the offset bias.

Due to the progressiveness of convolution and pooling, CNN has high robustness to overcome the objects' transformation of translation, tilting and displacement [15,16], which was perfectly suitable to solve the problem of change in the aggregates' shapes. To handle complex shapes and sizes in images, one localization CNN and five AI CNNs with different sized kernels were designed to complete the processes of evaluating the aggregates' AI in batches using images. First, a localization CNN was realized to locate and abstract each aggregate from images. Then, the image of each single aggregate was imported to five AI CNNs with different sized

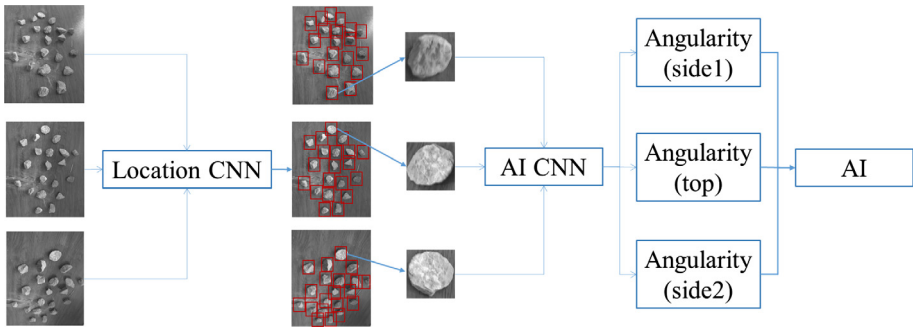

Fig. 4. Flow chart of CNN system.

kernels to evaluate the aggregates' AI. The processes are shown in Fig. 4. Meanwhile, the main processes of developing a CNN are similar to that shown in Fig. 5.

2.3.1. Localization convolutional neural network

In the past decade, CNN has been widely used in the field of localization object, such as traffic sign, human face and pedestrian [29–31]. Remarkably, CNN utilized in the field of localization is a mature method. Thus, it is a judicious plan to utilize CNN to locate and abstract each aggregate from the images of all viewpoints.

(a) The structure of CNN. One localization CNN was designed to realize this aim. The structural details of the localization CNN are shown in Fig. 6.
(b) The training of CNN. The training sample included 1500 images (500 images for the top side, 500 images for the left side, 500 images for the right side) and each image included 20 aggregates. Meanwhile, the target sample was the central coordinates of the bounding boxes, which are represented by the red boxes shown in Fig. 6. Notably, the size of the bounding boxes was 128 × 128 pixels. Stochastic gradient descent using 100 images in iteration was utilized in the training. To evaluate the results of training, the error of the central coordinates was calculated by formula (5).

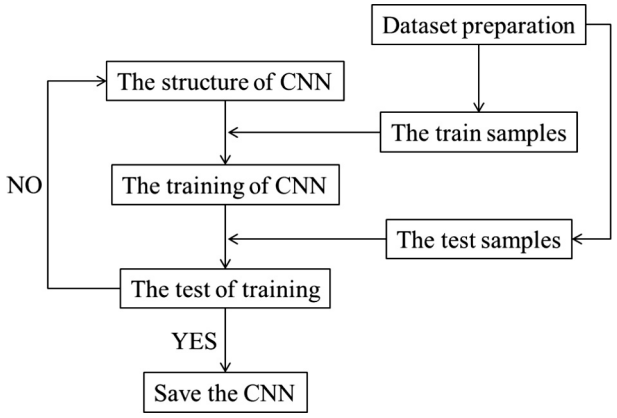

Fig. 5. Process of developing a CNN.

(c) The testing of CNN. 100 images for each direction (the top, left and right sides of aggregates) were included in a testing sample. Meanwhile, the target sample was the central coordinates of the bounding boxes, which were the same as those of the training sample. To evaluate the results of the testing, the error of the central coordinates was calculated by formula (5).

The processes mentioned above were realized based on Caffe using Intel(R) Core(TM) i7-6700 CPU, 8.00 GB Random Access Memory (RAM) and NVIDA GeForce GTX 1060 6 GB GPU. After training and testing for the localization CNN, all 1500 images were imported to the well-trained CNN to extract single aggregate images, and the images were used as the training and testing samples of AI CNNs.

$$error = \frac{\sqrt{(x - x')^2 + (y - y')^2}}{64} \tag{5}$$

2.3.2. AI convolutional neural network

CNN was also used to evaluate the AI from the images of all viewpoints. The steps were as follows:

(a) The structure of CNN. The aim of AI CNN is to build a relationship between single aggregate images and AI. However, CNN is used as classifiers without the regression function generally. To build the relationship, the traditional structure of CNN was changed by replacing the softmax layer with EuclideanLoss layer, which was used to calculate the error as shown in formula (6). Based on the EuclideanLoss layer, the structural details of AI CNNs are shown in Fig. 7. Five different sizes of kernels, i.e., 2 × 2, 4 × 4, 6 × 6, 8 × 8 and 10 × 10, were selected to design the AI CNNs because the size of the kernels influences the accuracy of the results.
(b) The training of CNN. 24000 single aggregate images for each direction (the top, left and right sides of aggregates) were included in the training sample. To ensure the robustness of AI CNNs, the aggregate images for the training sample included different sizes and textures of aggregates in different light conditions. The target sample was the AI computed by formulas (1) and (2), and stochastic gradient descent using 1200 images in iteration was utilized in the training.

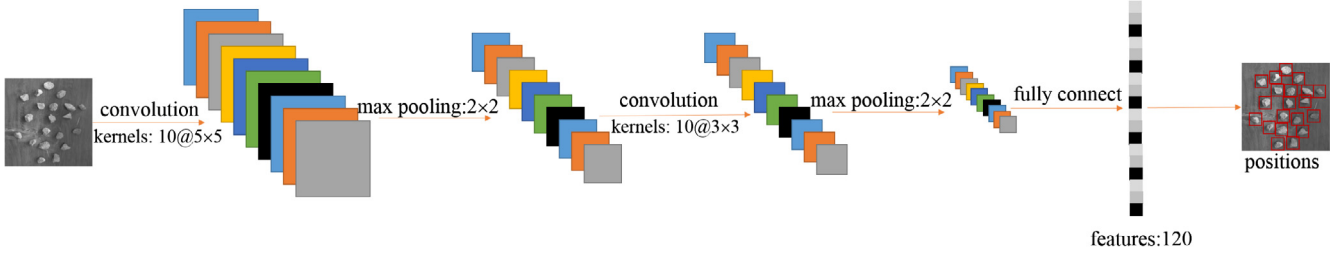

Fig. 6. Structure of localization CNN.

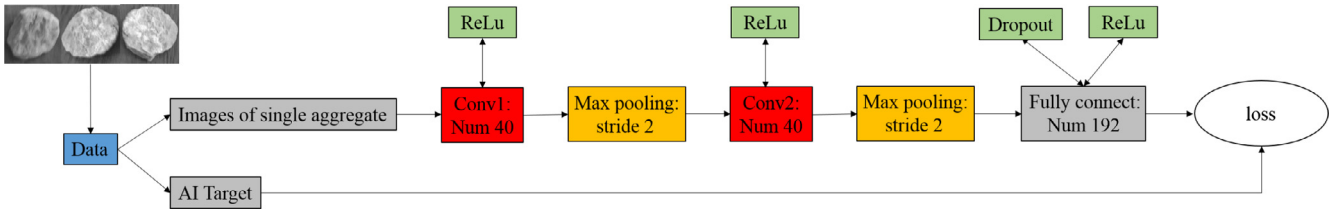

Fig. 7. Structure of AI CNN.

(c) The testing of CNN. 900 images for 100 single aggregates were established as the testing sample. The image for single aggregate was taken by the three viewpoints under three light conditions (dark, medium and bright).

The processes above were realized based on Caffe with Inter(R) Core(TM) i7-6700 CPU, 8.00 GB Random Access Memory (RAM) and NVIDA GeForce GTX 1060 6 GB GPU.

$$error = \frac{1}{2N}\sum_{n=1}^{N}\|y'_n - y_n\|_2^2 \quad (6)$$

2.4. Sensitivity analysis

Due to the effect of kernel sizes, image resolution, light condition and aggregate size and texture on the results of AI CNN, a statistical analysis for seeking the optimal AI CNN parameters, especially the sizes of kernel, and verifying the sensitivity of AI CNN was conducted. The analysis included sensitivity to sizes of kernels, image resolution, light, texture and size of aggregates. In all of the sensitivity analyses, two indexes, i.e., the shapes of box plots and relative errors, were utilized to analyze the sensitivity. The box plot is a great method to describe differences between different groups of data by comparing the shapes of box plots [13,32]. In this study, the shapes of box plots were adopted to analyze the global stability of AI values with one parameter changing. In addition, relative errors were adopted to evaluate the deviations between the real values of AI and the results given by AI CNNs.

(a) Sensitivity to sizes of kernels

One factor that needed to be considered after designing the general structure was the size of kernels. In this study, five different sizes of kernels, i.e., 2×2, 4×4, 6×6, 8×8 and 10×10, were used to determine the sensitivity to the sizes of kernels. A reasonable size of kernels was determined by analysis. Then, the reasonable size of kernels was selected for the rest of the sensitivity analysis.

(b) Sensitivity to image resolution

After selecting the kernel size, the image resolution should be determined. Five different PPIs (36 PPI, 54 PPI, 72 PPI, 180 PPI, 300 PPI) were used to evaluate the sensitivity to image resolution. To obtain these five PPIs, the parameters of the self-developed device were changed to acquire 36 PPI, 54 PPI, 72 PPI, 180 PPI and 300 PPI, respectively, to realize the aim of sensitivity analysis towards image resolution and to ensure the rationality of comparison among the five datasets.

(c) Sensitivity to light

To verify the robustness of AI CNN to different light conditions, two LEDs were adopted to simulate the light conditions of dark (0.1–100 *lx*), medium (100–400 *lx*) and bright (400–1000 *lx*) to capture the aggregate images for the training sample and the testing sample. In the sensitivity analysis to light, the testing sample was divided by the light conditions. The AI results of the same single aggregate in three different conditions were discussed to verify the robustness of AI CNN towards light.

(d) Sensitivity to size and texture of aggregate

The aggregate types of granite, basalt, marble and limestone with sizes of 3–5 mm, 5–10 mm and 10–15 mm were selected to study the robustness of the AI CNN to different sizes and texture of aggregates. Notably, the number of each type of aggregate was 25 in the testing sample, and the numbers of the sizes of 3–5 mm, 5–10 mm and 10–15 mm were 40, 30 and 30 separately.

3. Results and discussion

3.1. Performance of localization convolutional neural network

The localization CNN is responsible for aggregate location and abstraction of aggregate from images. Two indexes were used to estimate the performance of the localization CNN after each iteration. The first one is the central coordinates errors of bounding boxes described in 2.3.1, which were utilized to ensure that each aggregate was encircled by 128×128 pixel boxes. Then, the 128×128 pixel images were used as the training and testing samples of AI CNN. However, the numbers of aggregates detected were not estimated by the central coordinate errors. Thus, a second index called 'recall' was used to offset the disadvantage of the central coordinate errors. The definition of recall in the localization was the ratio between the number of aggregates given by the localization CNN and the real number of aggregates in the image, which was 20 in this study.

The result of training is shown in Fig. 8. Notably, the outputs were stable after 300 times of iteration, which indicated that the CNN located aggregates correctly with 0.99905 pixel of the central coordinates errors and 100% recall. After training, the testing sample was imported to the well-trained CNN to further verify the accuracy. The testing results showed that the location was correct with only 1.041 pixel of the central coordinates errors and 100% recall. Therefore, the training and testing CNN are desirable for the follow-up study. A procedural image from the testing as an output result of the second convolutional layer is shown in Fig. 9. Obviously, the consequences of convolutional layers were useful to locate the aggregate and even to evaluate the AI, due to the information of outlines remaining compared with the original image.

3.2. Performance of AI convolutional neural network

3.2.1. AI estimation with different sizes of kernels

As mentioned before, the results of AI given by the AI CNNs were mainly influenced by the sizes of kernels. Therefore, the results given by CNNs with kernel sizes of 2×2, 4×4, 6×6, 8×8 and 10×10 separately were discussed to determine the optimal size of kernels. Notably, two convolutional layers in one CNN

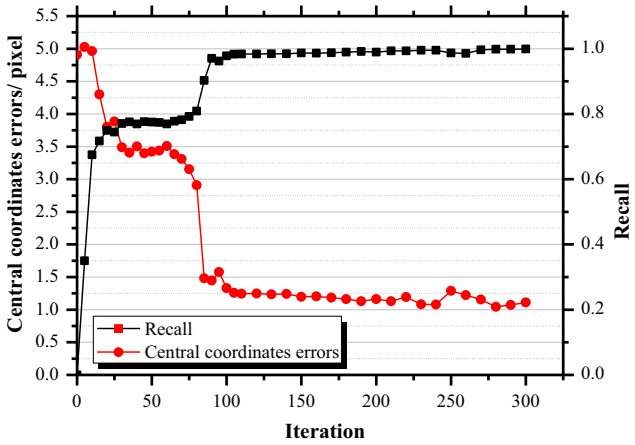

Fig. 8. Training results of AI CNN.

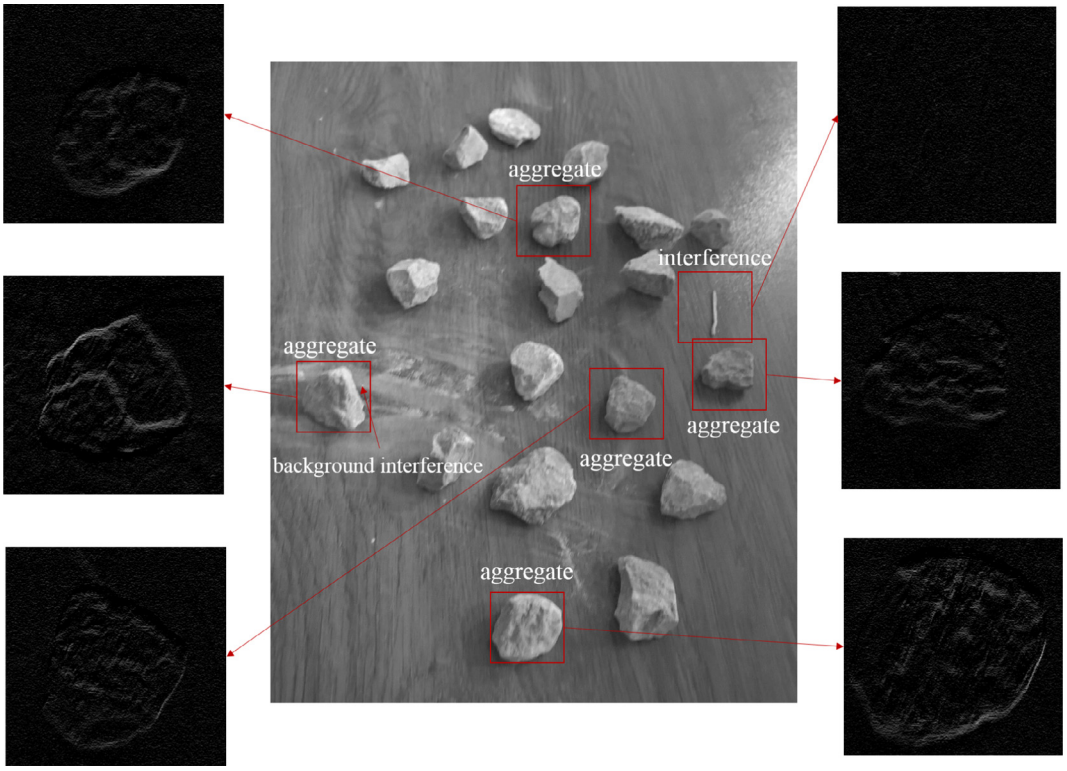

Fig. 9. Partial results of a process image.

had the same sized kernels. In this study, box plots were adopted to analyze the AI values. The AI results of 100 aggregates with different sized kernels are shown in Fig. 10. As shown in Fig. 10, the results of 6×6, 8×8 and 10×10 were close to each other in terms of the shapes of box plots, and the results were obviously different among 2×2, 4×4 and others. More accurately, the AI value ranges within the interquartile ranges (the 1st quartile subtracted from the 3rd quartile, also named as the lengths of boxes in the box plot) were 391–548, 398–537, 407–520, 438–543 and 435–520 for 2×2, 4×4, 6×6, 8×8 and 10×10 sized kernels, respectively. The changes of interquartile ranges exhibited lower values when the sizes of kernels became larger. Therefore, with the increment of the sizes of kernels, the outputs of AI CNNs became more stable (from 2×2 sized kernels, to 6×6 sized kernels, and up to 10×10). Relative error was used to evaluate the accuracy of different CNNs. The relative errors among 2×2, 4×4, 6×6, 8×8 and 10×10 sized kernels were 0.1477, 0.1228, 0.0938, 0.0874 and 0.0802. The AI values became close to the target sample as the kernel size became larger. Therefore, with the increment of the sizes of kernels, the outputs of AI CNNs became more accurate. The accuracies of 6×6, 8×8 and 10×10 sized kernels were all acceptable.

The main reason for this was that with the increasing size of kernels, the values of two neighboring pixels would be closer, decreasing the error in the pooling operation. In addition, this could be the reason that a smaller sized kernel would be more sensitive to the surroundings. Additionally, it should be noticed that a larger sized kernel led to the increment of parameters, which easily caused overfitting in some values. Thus, the sizes of kernel should be controlled in a reasonable range.

Meanwhile, the calculation efficiency was also considered, where the accuracies of 6×6, 8×8 and 10×10 sized kernels were

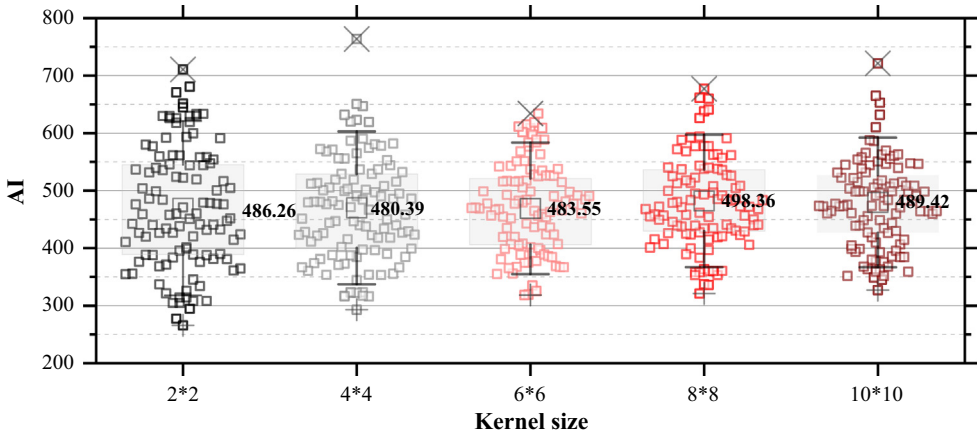

Fig. 10. Box plot for AI CNN with five kernel sizes.

all acceptable. The computational times for 6×6, 8×8 and 10×10 sized kernels in computing the AI values of the testing sample were 825 ms, 1343 ms and 1792 ms, respectively, which means that a larger sized kernel would increase the computation load dramatically.

Therefore, the AI CNN with 6×6 sized kernels was utilized for the rest of the sensitivity analysis because it exhibited optimal accuracy and efficiency for evaluating the AI. However, only the condition of two convolutional layers having the same sized kernels was considered in this study. The condition of kernels that have different sizes in two convolutional layers should be determined to further improve the accuracy and efficiency of CNN in a future work.

3.2.2. AI estimation with different resolutions

After determining the size of kernels, sensitivity analysis of the image resolution was performed by using the AI CNN with 6×6 sized kernels. The AI results of 100 aggregates with different image solutions of 36 PPI, 54 PPI, 72 PPI, 180 PPI and 300 PPI are shown in Fig. 11. To obtain the other four PPIs, the parameters of the self-developed device were changed to acquire 36 PPI, 54 PPI, 72 PPI, 180 PPI and 300 PPI, respectively, to realize the aim of sensitivity analysis towards image resolution and ensure the rationality of the comparison among the five datasets.

As shown in Fig. 11, the results of 72 PPI, 180 PPI and 300 PPI were close from the shapes of box plots, and the results were obviously different among 36 PPI, 54 PPI and others. More accurately, the AI value ranges within the interquartile ranges were 392–552, 402–545, 413–541, 418–539 and 405–515 for 36 PPI, 54 PPI, 72 PPI, 180 PPI and 300 PPI, respectively. The changes of interquartile ranges were lower as well when the image resolution became larger. Therefore, with the increment of image resolution, the outputs of AI CNNs became more stable (from 36 PPI, to 72 PPI, and up to 300 PPI). Thus, in the range of 72–300 PPI, the AI CNN with 6×6 sized kernels had great robustness to image resolution. Relative error was used to evaluate the accuracy of different resolutions. The relative errors among images resolutions of 36 PPI, 54 PPI, 72 PPI, 180 PPI and 300 PPI were 0.1570, 0.1248, 0.1006, 0.0945 and 0.0938. Therefore, with the increment of image resolution, the outputs of AI CNNs became more accurate. Thus, we could conclude that there was no significant influence of images resolution in the range of 72–300 PPI. However, low resolution images in the range of 36–72 PPI showed bad performance in the evaluation of AI.

The reason why low resolution images had a negative influence on the work of AI CNN is that with the decrease of pixel dots in one inch, less details on angularity remained after the convolutional operation and even some negative changes happened in the field of the aggregates' edges. With the loss of some important feature information, the regression results in fully connected layers and EuclideanLoss layer easily deviated from the actual results.

3.2.3. AI estimation with different light conditions

After determining the size of kernels, sensitivity analysis to different light conditions was conducted by using the AI CNN with 6×6 sized kernels and 300 PPI image resolution.

The AI results of 100 aggregates with different light conditions, i.e., bright, medium and dark, are shown in Fig. 12. As shown in Fig. 12, the results of three different conditions were close from the shapes of box plots. More accurately, the AI value ranges within the interquartile ranges were 407–520, 403–530 and 410–535 for bright, medium and dark conditions, respectively. The changes of interquartile ranges were lower in the three different conditions. Therefore, the outputs of AI CNNs were stable under the different light conditions. One aggregate image in these three conditions after the convolution operation is shown in Fig. 12. The information of particle outlines mainly remained, which was the necessary detail for fully connection layers to realize the regression calculation. Other unnecessary information such as textures and shadow was removed perhaps. Consequently, 6×6 sized kernels, whose parameters were shared by sub-windows in each kernel and were different with each other internally, showed the capacity to address different light conditions. In addition, relative error was also used to evaluate the accuracy of different light conditions. The relative errors among bright, medium and dark conditions were 0.0938, 0.0976 and 0.0996, which were also close to each. Based on Fig. 12 and the relative errors, we could conclude that there was no significant influence of light in the range of 0.1–1000 *lx* on the outputs of AI CNN with 6×6 sized kernels. Moreover, the range of 0.1–1000 *lx* covered the lightest conditions in the working conditions. However, light was necessary for digital cameras to image.

3.2.4. AI estimation with different aggregate shapes and textures

As mentioned before, to verify the robustness of AI CNN to different sizes and textures of aggregates, granite, basalt, marble and limestone were included in the testing sample of aggregate images. The different types of aggregates had different textures. In addition, three sizes, i.e., 3–5 mm, 5–10 mm and 10–15 mm, were included in the testing sample of aggregate images. In the sensitivity analysis towards sizes and textures, the testing sample was divided by the type and sizes of aggregates. The AI results of the same single aggregate in type and sizes were discussed to verify the robustness of AI CNN. Notably, the number of each type of

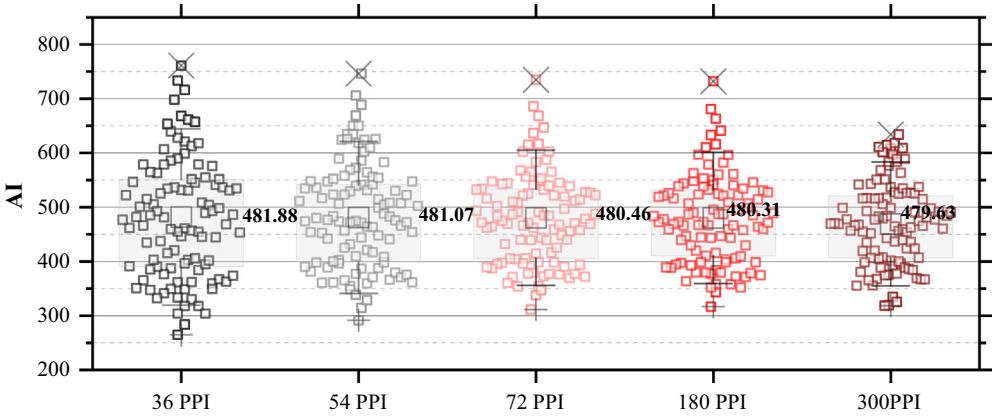

Fig. 11. Box plot for AI CNN with five different PPIs.

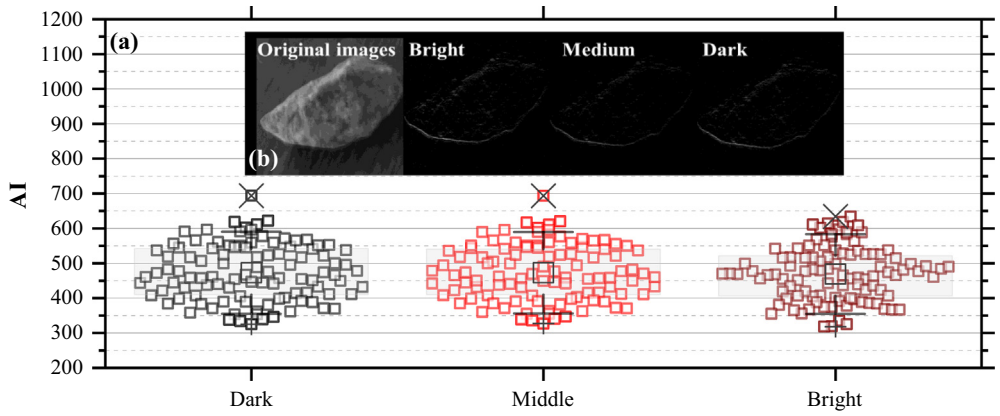

Fig. 12. Box plot for AI CNN with different light conditions.

aggregate was 25 in the testing sample, and the numbers of sizes of 3–5 mm, 5–10 mm and 10–15 mm were 40, 30 and 30.

The AI results of 100 aggregates with different textures are shown in Fig. 13. As shown in Fig. 13, the results of different textures were close from the shapes of box plots. More accurately, the AI value ranges within the interquartile ranges were 468–591, 403–510, 401–509 and 360–469 for granite, basalt, marble and limestone, respectively. The changes of interquartile ranges were low values. Therefore, the outputs of AI CNNs were stable for calculating AI values for different textures (granite, basalt, marble and limestone). Relative error was used to evaluate the accuracy of different textures. The relative errors among granite, basalt, marble and limestone were 0.0821, 0.1085, 0.0872 and 0.0971. Therefore, the outputs of AI CNNs were accurate for different textures (granite, basalt, marble and limestone). Obviously, we could conclude that there was no significant influence of different textures. However, compared with the other three types of aggregates, the relative errors of basalt were larger, even though these relative errors were acceptable. The reason why basalt had a negative influence on the work of AI CNN was that the colors of basalt included in the testing samples were partially black, causing some details to be unrecognized. With the loss of details, fewer details on

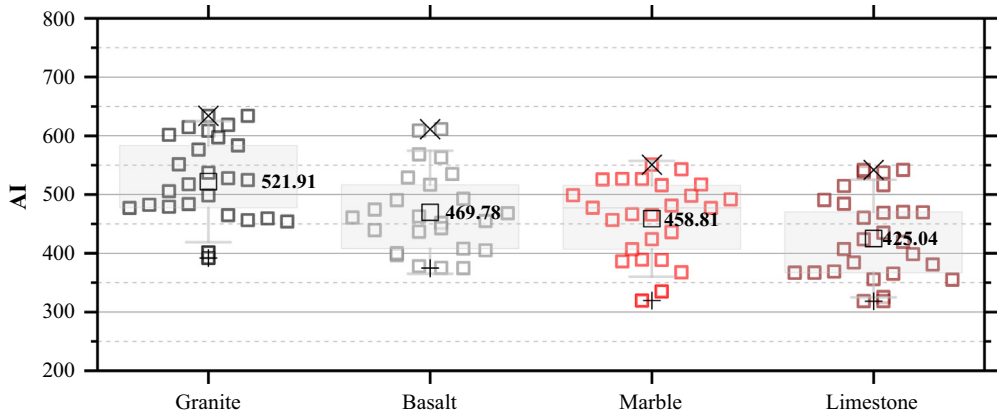

Fig. 13. Box plot for AI CNN with different textures.

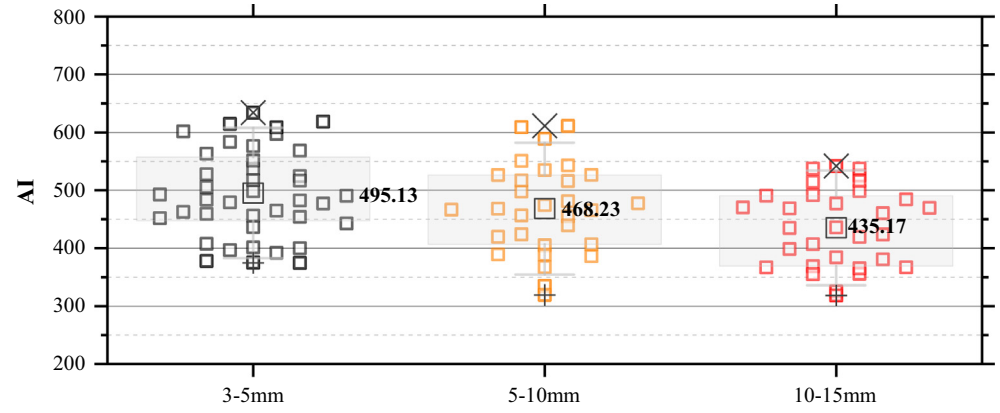

Fig. 14. Box plot for AI CNN with different sizes.

angularity remained after the convolutional operation and even some negative changes happened in the field of the aggregates' edges. With the loss of some important feature information, the regression results in fully connected layers and EuclideanLoss layer easily deviated from the actual results.

The AI results of 100 aggregates with different sizes are shown in Fig. 14. As shown in Fig. 14, the results of different sizes were close from the shapes of box plots. More accurately, the AI value ranges within the interquartile ranges were 449–554, 405–527 and 360–493 for 3–5 mm, 5–10 mm and 10–15 mm, respectively. The changes of interquartile ranges were lower values. Therefore, the outputs of AI CNNs were stable for calculating AI values for different sizes (3–5 mm, 5–10 mm, 10–15 mm). The relative errors among sizes of 3–5 mm, 5–10 mm and 10–15 mm were 0.0953, 0.0931 and 0.0925. Obviously, we could conclude that there was no significant influence of the different sizes in the range of 3–15 mm on the output accuracy of the AI CNN based on Fig. 14 and relative errors. However, compared with the three other sizes, the relative errors of 3–5 mm were larger, even though these relative errors were acceptable. The reason why the size of 3–5 mm had a negative influence on the work of AI CNN was that aggregates with size of 3–5 mm showed less details in each inch. With the decrease of the pixel dots in one inch, less details on angularity remained after the convolutional operation in the field of the aggregates' edges. With the loss of some important feature information, the regression results in fully connected layers and EuclideanLoss layer easily deviated from the actual results.

4. Conclusions

The application of CNN using digital images for evaluating the aggregate angularity was presented in this study, and the following conclusions can be drawn:

(1) Based on the view-based approach, a self-developed device for acquiring aggregate images was developed. Because of the angle θ in the imaging cameras, a self-developed device was more reasonable for detecting several aggregates at the same time.
(2) After a comparison among different factors under consideration, 6×6 sized kernels were selected as the optimal way to evaluate AI. This was mainly because the AI CNN with 6×6 sized kernels was less sensitive to the border of aggregates and the surroundings. To further utilize the AI CNN, the PPI of the acquired image should be more than 72.
(3) Sensitivity analysis to image resolution showed that there was no significant influence of images resolution in the range of 72–300 PPI. Sensitivity analysis to different light conditions, sizes and textures of aggregates showed that there were no significant influences of these on AI CNN with 6×6 sized kernels.
(4) The AI CNN with 6×6 sized kernels was the most acceptable due to its relative error of 0.0938 and computational time of 825 ms for computing the AI values of the testing sample. Though the relative errors of AI CNN with 8×8 and 10×10 sized kernels were lower than that of the AI CNN with 6×6 sized kernels, their computational times were increased dramatically to 1343 ms and 1792 ms, respectively, which may not be an acceptable efficiency for AI evaluation.
(5) The relative errors of the AI CNN with 6×6 sized kernels among bright, medium and dark conditions were 0.0938, 0.0976 and 0.0996, and the relative errors among granite, basalt, marble and limestone were 0.0821, 0.1085, 0.0872 and 0.0971. The relative errors among aggregate sizes of 3–5 mm, 5–10 mm and 10–15 mm were 0.0953, 0.0931, 0.0925. All of these showed that the AI CNN with 6×6 sized kernels had great stability for these light conditions, sizes and textures of aggregates.
(6) Only the condition of two convolutional layers having the same sized kernels was considered in this study. The condition of kernels that have different sizes in two convolutional layers should be determined to further improve the accuracy and efficiency of CNN in future work.

Acknowledgements

The authors gratefully appreciate the supports from the key laboratory of road in Chang'an University and Northeast Forestry University and the foundations for the project of Heilongjiang Traffic and Transportation Department.

References

[1] M.E. Kutay, H.I. Ozturk, A.R. Abbaa, C. Hu, Comparison of 2D and 3D image based aggregate morphological indices, Int. J. Pavement Eng. 12 (4) (2011) 421–431.
[2] E. Tutumluer, T. Pan, Aggregate morphology affecting strength and permanent deformation behavior of unbound aggregate materials, J. Mater. Civil Eng. 20 (9) (2008) 617–627.
[3] R.D. Barksdale, C.O. Pollard, T. Siegel, S. Moeller, Evaluation of the Effects of Aggregate on Rutting and Fatigue of Asphalt. Research Report. Georgia DOT Project 8812, GA Tech Project E20-835, Georgia Institute of Technology, Atlanta, 1992.
[4] T.W. Kennedy, G.A. Huber, E.T. Harrigan, R.J. Cominsky, C.S. Hughes, H. Von Quintus, J.S. Moulthrop, Superior Performing Asphalt Pavements (Superpave®). The product of the SHRP Asphalt Research Program. SHRP-A-410, TRB, National Research Council, Washington, D.C., 1994.
[5] Leonardo T. Souza, Yong-Rak Kim, A.M. ASCE, Flavio V. Souza, Leandro S. Castro, Experimental testing and finite-element modeling to evaluate the effects of aggregate angularity on bituminous mixture performance, J. Mater. Civil Eng. 24 (3) (2012) 249–258.
[6] D. Singh, M. Zaman, S. Commuri, Inclusion of aggregate angularity, texture, and form in estimating dynamic modulus of asphalt mixes, Road Mater. Pavement Des. 12 (2) (2012) 327–344.
[7] T.A.N. Yi-qiu, S.O.N.G. Xian-hui, J.I. Lun, C.H.E.N. Guo-ming, W.U. Xiao-ting, Influence of coarse aggregate performance on high temperature performance of asphalt mixture, China J. Highway Transport 22 (1) (2009) 29–33.
[8] JTG E42-2005, Test Methods of Aggregate for Highway Engineering.
[9] AASHTO T326-05(2009), Standard Method of Test for Uncompacted Void Content of Coarse Aggregate (As Influenced by Particle Shape, Surface Texture, and Grading).
[10] ASTM D3398—2000, American Society for Testing and Materials Standards.
[11] E. Masad, The Development of a Computer Controlled Image Analysis System for Measuring Aggregate Shape Properties, in NCHRP-IDEA Project 77, National Research Council, Washington, 2003.
[12] E. Tutumluer, C. Rao, J.A. Stefanski, Video image analysis of aggregates, FHWA-IL-UI-278, 2000.
[13] Xu. Siyu Chen, Zhanping You Yang, Min Wang, Innovation of aggregate angularity characterization using gradient approach based upon the traditional and modified Sobel operation, Constr. Build. Mater. 120 (2016) 442–449.
[14] Bian Xuecheng, Li Gongyu, Li Wei, Jiang Hongguang, Morphology analysis of coarse aggregate based on 3D imaging method by using two planar mirrors, China Civil Eng. J. 47 (9) (2014) 135–144.
[15] Yu. Biao Leng, Kai Yu Liu, Xiangyang Zhang, Zhang Xiong, 3D object understanding with 3D convolutional neural networks, Inf. Sci. (2015) 1–14.
[16] S. Ji, W. Xu, M. Yang, K. Yu, 3D convolutional neural networks for human action recognition, IEEE Trans. Pattern Anal. Mach. Intell. 35 (1) (2013) 221–231.
[17] H. Lee, P. Pham, Y. Largman, A. Ng, Unsupervised feature learning for audio classification using convolutional deep belief networks, Proc. Adv. Neural Inf. Process. Syst. (2009) 1096–1104.
[18] V. Jain, J.F. Murray, F. Roth, S. Turaga, V. Zhigulin, K.L. Briggman, M.N. Helmstaedter, W. Denk, H.S. Seung, 2007. Supervised learning of image restoration with convolutional networks, in: Proceedings 11th IEEE Int'l Conference Computer Vision.
[19] V. Jain, S. Seung, Natural image denoising with convolutional networks, Proc. Adv. Neural Inf. Process. Syst. 21 (2009) 769–776.
[20] S.C. Turaga, J.F. Murray, V. Jain, F. Roth, M. Helmstaedter, K. Briggman, W. Denk, H.S. Seung, Convolutional networks can learn to generate affinity graphs for image segmentation, Neural Comput. 22 (2) (2010) 511–538.
[21] R. Osada, T. Funkhouser, B. Chazelle, D. Dobkin, Shape distributions, ACM Trans. Graphics 21 (4) (2002) 807–832.

[22] G. Patane, M. Spagnuolo, B. Falcidieno, A minimal contouring approach to the computation of the Reeb graph, IEEE Trans. Visualization Comput. Graphics 15 (4) (2009) 583–595.
[23] J.-L. Shih, C.-H. Lee, J.T. Wang, A new 3D model retrieval approach based on the elevation descriptor, Patt. Recognit. 40 (1) (2007) 283–295.
[24] M. Chaouch, A. Verroust-Blondet, 3D model retrieval based on depth line descriptor, in: Proceedings of the IEEE International Conference on Multimedia and Expo, Beijing, China, 2007, pp. 599–602.
[25] P. Daras, A. Axenopoulos, A 3D shape retrieval framework supporting multimodal queries, Int. J. Comput. Vision 89 (2) (2010) 229–247.
[26] Y. Gao, M. Wang, D.-C. Tao, R.-R. Ji, Q.-H. Dai, 3D object retrieval and recognition with hypergraph analysis, in: IEEE transactions on image processing, 2012, 21(9):4290–4303. 21 (9) (2012) 4290– 4303.
[27] B. Leng, Z. Xiong, Modelseek: an effective 3D model retrieval system, Multimedia Tools. Appl. 51 (3) (2011) 935–962.
[28] Chetana Rao, Erol Tutumluer, In Tai Kim, Quantification of coarse aggregate angularity based on image analysis, Transp. Res. Record J. Transp. Res. Board 1787 (1) (2002) 117–124.
[29] Yingying Zhu, Chengquan Zhang, Duoyou Zhou, Xinggang Wang, Xiang Bai, Wenyu Liu, Traffic sign detection and recognition using fully convolutional network guided proposals, Neurocomputing 214 (2016) 758–766.
[30] Yuan Dong, Wu. Yue, Adaptive cascade deep convolutional neural networks for face alignment, Comput. Stand. Interfaces 42 (2015) 105–112.
[31] D. Tomè, F. Monti, L. Baroffio, L. Bondi, M. Tagliasacchi, S. Tubaro, Deep convolutional neural networks for pedestrian detection, Signal Processing: Image Commun. 47 (2016) 482–489.
[32] Q. Lu, J. Harvey, R. Wu, Investigation of Noise and Durability Performance Trends for Asphaltic Pavement Surface Types: Four-Year Results, Univ. of California, Davis, CA, 2011.